Enhanced thermoelectric performance of n-Type Bi$_2$S$_3$ added with ZnO for power generation

Xueli Du,*[a] Rongna Shi,[a] Yongchang Ma,[b] Fengshi Cai,[b] Xuewei Wang,[c] and Zhihao Yuan[c]

Abstract: Although Bi$_2$S$_3$ is one of promising thermoelectric materials, the practical application is limited by relatively low dimensionless figure of merit (*ZT*), especially low electrical conductivity. In this work, ZnO was used to tune thermal and electrical properties of Bi$_2$S$_3$. In the preparation process of mechanical alloying (MA) and spark plasma sintering (SPS), small amount of ZnO converted to ZnS in the sulfur rich environment and accompanied with the production of sulfur vacancies and micro/nanostructures. The sulfur vacancies increased the electrical conductivity of n-Type Bi$_2$S$_3$ and micro/nanostructures scattered phonons without commonly deteriorating electronic transport. The maximum *ZT* value of 0.66 at 675 K for Bi$_2$S$_3$ doped with 1.0 mol% ZnO was obtained and the results of this work perhaps provide a new way for designing and fabricating thermoelectric materials.

Keywords: Bismuth sulfides, Zinc oxide, Thermoelectric, Sulfur vacancy, Micro/nanostructure

Introduction

Bismuth sulfide (Bi$_2$S$_3$, without toxic and scarce tellurium element) is a promising thermoelectric (TE) material for its high Seebeck coefficient and low thermal conductivity, as an n-type semiconductor the carrier electrons generate from the sulfur deficiencies,[1-3] but the direct bandgap of around 1.3 eV results in the low electrical conductivity.[4]

[a]School of Materials Science & Engineering, Tianjin University of Technology, Tianjin 300384, China. E-mail: d7288@126.com; Tel: +86-22-60216936

[b]Tianjin Key Lab for Photoelectric Materials & Devices, Tianjin University of Technology, Tianjin 300384, China

[c]Key Laboratory of Display Materials & Photoelectric Devices (Tianjin University of Technology), Ministry of Education, Tianjin 300384, China

Many efforts have been made to increase electrical conductivity. L. D. Zhao[5] made the sub-stoichiometric Bi_2S_{3-x} bulks and the electrical conductivity was increased from 10^0 S cm^{-1} to 10^2 S cm^{-1} by tailoring the sulfur content. Y. Q. Yu[6] and Z. H. Ge[7, 8] also increased the electrical conductivity of Bi_2S_3 bulks by doping Ag and Cu or orientation nanorods. In the work of K. Biswas, the electrical conductivity of oriented Bi_2S_3 ingots doped with $BiCl_3$ was increased to 615 S cm^{-1} at room temperature along the ingot growth direction, but the thermal conductivity was increased accordingly.[9]

As an assessment parameter of thermoelectric conversion efficiency, *ZT* is associate with Seebeck coefficient (α), electrical conductivity(σ), thermal conductivity (κ) and absolute temperature (T), according to equation $ZT = \frac{\alpha^2 \sigma}{\kappa} T$.[10] In order to achieve high *ZT*, high power factor (PF, $\alpha^2\sigma$) and low thermal conductivity are required. For improving PF, the doping technology was used for tuning carrier concentration,[11] but the carrier concentration and the effective mass has the opposite effect on σ and α or κ.[12] From Mott expression and Mahan-Sofo theory, α is increased with density of states (DOS) at the Fermi energy,[13-15] therefore, modifying the DOS[14, 16] and converging valence (or conduction) bands[17, 18] for enhancing α have been made great progress on telluride thermoelectric materials. Thermal conductivity includes carrier transporting (κ_e) and phonon of lattice vibration (κ_l) components ($\kappa = \kappa_e + \kappa_l$). In comparison, more efforts have been made to reduce lattice thermal conductivity with phonon scattering mechanism by nonoscale grain boundaries [19-21] as well as phase separation.[22-24] In addition, some strategies such as mesopores and anti-resonant doping methods have attempted to apply all enhancement mechanisms to a single material.[15, 25, 26]

In this paper, zinc oxide (ZnO) was used to enhance electrical and thermal properties of n-type

Bi_2S_3. The bulk Bi_2S_3 added with x mol% ($x = 0\text{-}2.0$) ZnO was prepared by applying mechanical alloying (MA) and spark plasma sintering (SPS) techniques. The results reveal that the added ZnO can improve thermoelectric performance by sulfur vacancies and micro/nanostructures, and the *ZT* value is reaches 0.66 at 675 K by optimizing ZnO concentration.

Experiments

The commercial powders of bismuth (100 mesh, 99.5%, Aldrich), sulfur (100 mesh, reagent grade, Sigma-Aldrich) and ZnO ($< 1\mu m$, 99.9%, Aldrich) were used as raw materials. Bi_2S_3 added with x mol% ZnO ($x=0, 0.5, 1.0, 1.5, 2.0$) were synthesized by ball milling at 450 rpm for 15 h in argon atmosphere and the obtained powders were sintered at 773 K for 5 min in a $\Phi 20$ mm graphite mold under a mechanical pressure of 50 Mpa in vacuum with a SPS system (HPD 25/1 FCT Germany) and produced disk-shaped bulk samples. The bulk samples were cut and polished for further electrical and thermal properties characterization.

The phase composition of samples was analyzed using X-ray diffraction system (CuKα1, 1.54059 Å, X'Pert PRO, PANalytical) at room temperature. Scanning electron microscope (SEM) observation was carried out on JSM-6300 (JEOM, Japan) and transmission electron microscope (TEM) investigation was conducted under JEOL 2100 operated at 200 kV, TEM specimens were prepared by cutting, grinding, polishing and Ar-ion milling (Gatan 691, USA) procedure. Electrical conductivity and Seebeck coefficient were measured simultaneously under vacuum from room 300 K to 673 K on a thermoelectric measurement system (Namicro-Ⅱ, Wuhan, China), the typical samples for measurement had a rectangular shape with the dimensions of $\approx$ 3 mm $\times$ 3 mm $\times$ 14 mm. Thermal diffusivity (D) was directly measured and heat capacity (Cp) was indirectly derived using standard sample (Inconel) in the range 300-673 K using laser flash

method (LFA-457, Netzsch, Germany), disks with 10 mm diameter and $\approx$ 2 mm thickness were used in all the measurements.

Results and discussion

Fig. 1 shows the X-ray diffraction (XRD) patterns of sintered Bi_2S_3 bulks added with x mol% ZnO (x=0, 0.5, 1.0, 1.5, 2.0), All peaks confirm the orthorhombic Bi_2S_3 structure in the Pbnm space group but no visible impurity phase can be observed even as the x climbs to 2.0. The enlarged patterns in 2θ ranges 24-30º in figure 1b illustrate that the main diffraction peaks around 24.9 ° and 28.6 ° shift slightly to higher diffraction angle with increasing ZnO content, indicating the shrinkage of host lattice.
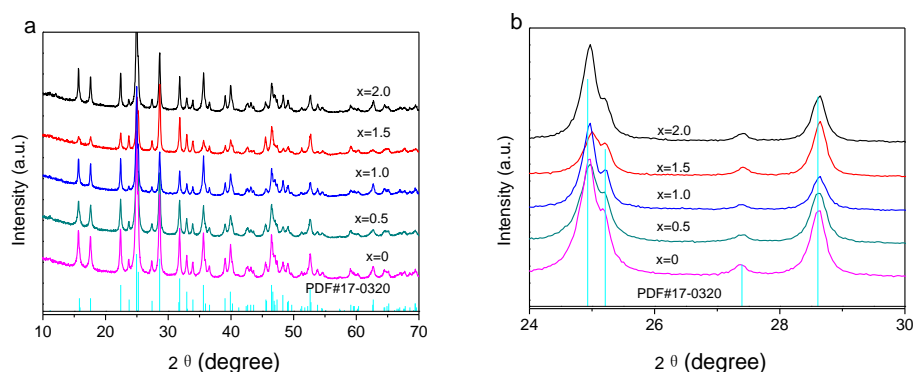
Fig.1 XRD patterns of sintered samples (a) and their enlarged patterns in 2θ ranges 20-30º (b) for Bi_2S_3 added with x mol% ZnO (x=0, 0.5, 1.0, 1.5, 2.0)

The TEM image in fig. 2a illustrates that the ultrafine Bi_2S_3 powders with a mean size about 30 nm produced by high-speed (450 rpm) MA process easily agglomerate into larger particles. The SEM morphology of the fractured surfaces for sintered bulk samples are shown in fig.2b-f. No obvious secondary phase can be found on the grain boundary, and the grain shows an orthorhombic lamellar structure with the thickness much less than 1 μm, which result from the

synthesized ultrafine powders and rapid SPS process. The relative density of Bi_2S_3 bulks added

with x mol% ZnO (x=0, 0.5, 1.0, 1.5, 2.0) are 95 %, 95.4 %, 95.8 %, 95.4 % and 94.6 %

respectively, indicates that the moderate amounts of ZnO (x<1.5) promoted the sintering

densification.
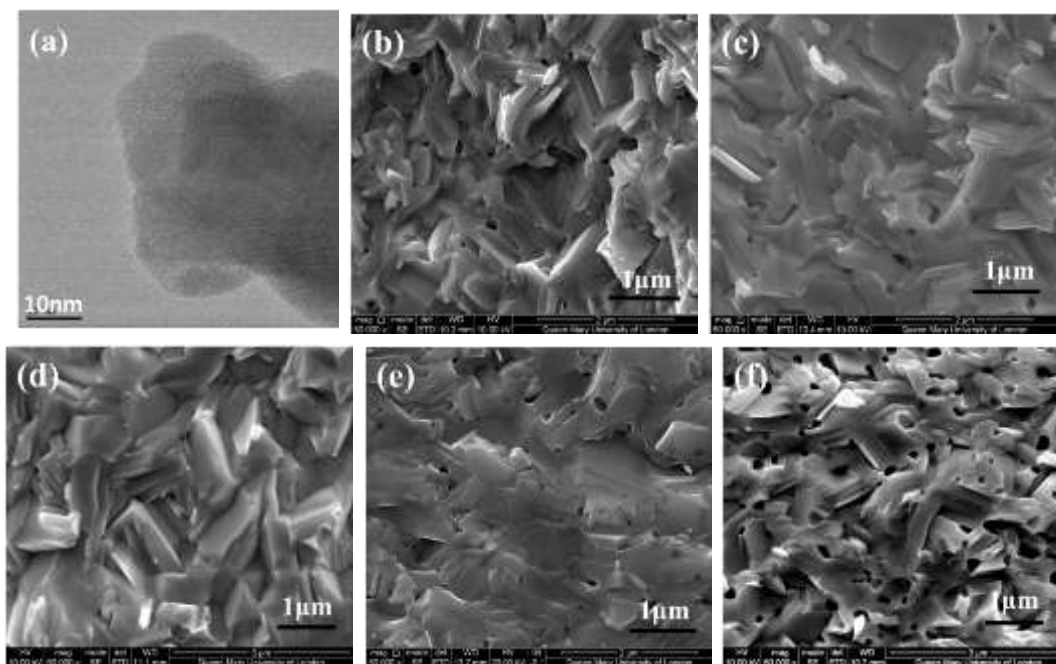
Fig. 2 TEM image of (a) synthesized Bi_2S_3 powder and SEM micrographs of (b-f) fractured

surfaces of sintered bulks for Bi_2S_3 added with x mol% ZnO (x=0, 0.5, 1.0, 1.5, 2.0)

In order to track the added ZnO, further investigations were conducted on TEM, fig. 3 is the

obtained images of Bi_2S_3 bulk added with 1.0 mol % ZnO. Fig. 3a is the low-magnification of the

sample, in which three different areas are observed and marked A, B and C. A is the area in the

grain, B and C are the areas at triple grain junctions and appear as bright "inclusions". Fig. 3b and

3c are the high-magnification and high-resolution images of area A, showing nanoscale particles

(5-10 nm) with different orientation and non-faceted with the matrix. In the selected area electron

diffraction (SAED) pattern of area A (inset of fig. 3b), only orthorhombic Bi_2S_3 Bragg spots can be

identified and illustrated that the Bi_2S_3 structure is not changed by added ZnO. The "inclusions"

on the grain boundaries (fig. 3a) are much thinner than the matrix and exhibit bright and there are

traces of gas expanded (fig. 3d) and some "inclusions" are broken (fig. 3e). The SAED of area B

(inset of fig. 3d) illustrates a mixture of hexagonal ZnS along $[1\bar{1}0]$ zone axe and orthorhombic

Bi_2S_3 along [010] direction.
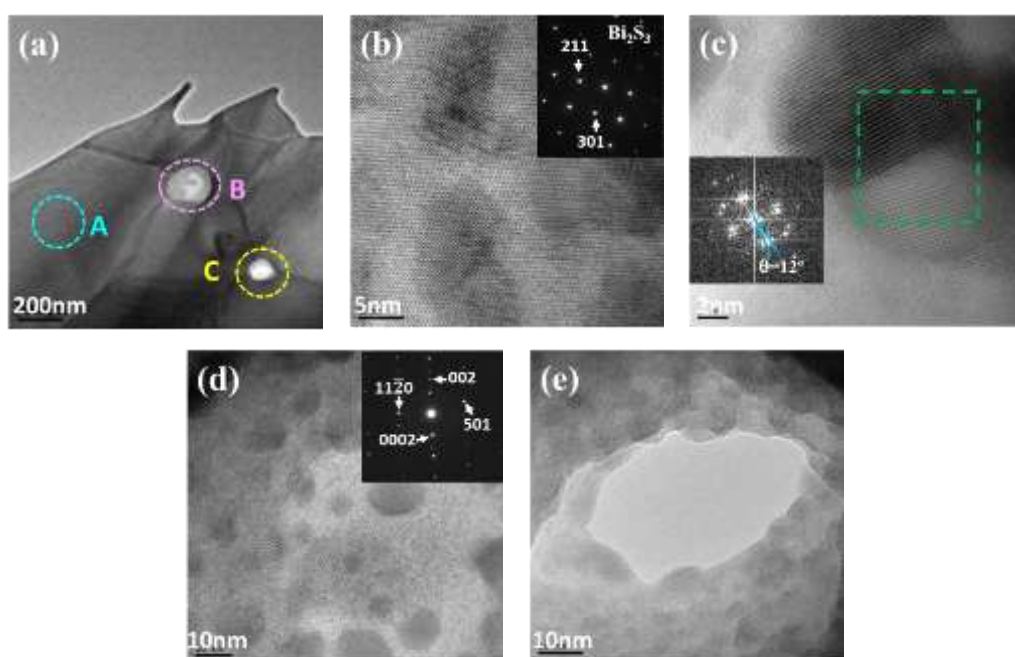
Fig. 3 TEM images of Bi_2S_3 added with 1.5 mol% ZnO. (a) Low-magnification revealing

typical areas A, B and C. (b) High-magnification of area A, inset is the SAED pattern along the

$[11\bar{3}]$ zone axe of Bi_2S_3. (c) High-resolution image of (b), showing the nanoscale particles (5-10

nm) with different orientation, inset is reduced FFT image from the marked area, revealing

high-angle (about 12°) boundary. (d) High-magnification of area B composed of nanoscale

precipitates (about 10 nm), the inset of SAED illustrating the $[1\bar{1}0]$ of hexagonal ZnS and [010] of

Bi_2S_3 zone axes. (e) High-magnification of area C, showing a broken nano bubble.

Thermodynamic calculations and research results review that ZnO will be reacted with

elementary sulfur and produced ZnS at higher temperature, the reaction as follows:[27-29]

$$2ZnO + 3S = 2ZnS + SO_2\uparrow \tag{1}$$

Under characteristic high-energy MA conditions, microstructures and substructures developed are conducive for initiating reactions that normally occur at elevated temperatures,[30] along with the subsequent SPS process, ZnO will be converted to ZnS in the sulfur rich environment, especially at high energy grain boundaries, which can reasonably explains the results in fig. 3d, e. Moreover, reaction (1) results in the sulfur vacancies in Bi_2S_3, which is probably the main reason for the lattice shrinkage of Bi_2S_3 added with ZnO, as shown in fig. 1b. Of course, the lattice shrinkage may also be induced by small radius Zn^{2+} (0.74 Å) substituted large radius Bi^{3+} (1.03 Å), but, as an electron acceptor, the doped Zn^{2+} will decrease carrier (electron) concentration and the defects in the cation sublattice will scatter electrons.[31] In fact, the electrical conductivity of Bi_2S_3 added with ZnO is increased (fig. 4a). From the view of sintering theory, the chemical reaction can also activate the sintering process and the production as secondary phase inhibits the grain growth, but the gas production will decrease the density of sintered sample, which consistent with the results of fig. 2b-f.

Fig. 4 is the temperature dependence of thermoelectric properties for Bi_2S_3 added with x mol% ZnO (x=0, 0.5, 1.0, 1.5, 2.0). The electrical conductivity (σ, fig. 4a) increases with increasing temperature for the samples of x=0 and 0.5, indicating a semiconductor conducting behavior. For semiconductor the electrical conductivity (σ) is directly proportional to carrier concentration (n), carrier charge (q) and carrier mobility (μ) according the formula $\sigma = nq\mu$. On account of the decreased carrier mobility at higher temperature, the σ value increases first and then decreases toward intrinsic value with increasing temperature after x>0.5. Furthermore, the σ value increases first and then decreases with increasing x, indicating the optimum doping concentration of ZnO is 1.0 mol%. During the MA and SPS processes, reaction (1) reduced the sulfur stoichiometric ratio

in Bi_2S_3 and resulted in sulfur vacancies $V_S^{\cdot\cdot}$ and free electrons ($e^{'}$), which can be described by the following equation:

$$x\ ZnO + 2Bi + 3S = x\ ZnS + Bi_2S_{3-1.5x} + 0.5\ x\ SO_2\uparrow + 1.5x\ V_S^{\cdot\cdot} + 3x\ e^{'} \qquad (2)$$
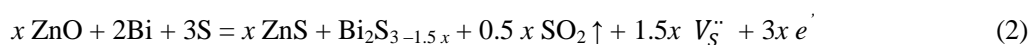
From above equation, the carrier (electron) concentration will increase with x increasing. Accordingly, the electrical conductivity also increases with x, but the σ values decreased after x>1.0, which attributes to the lattice and/or microstructure defects scattering the electrons. Compared with the reported sub-stoichiometric Bi_2S_{3-y} bulks,[5] the added ZnO not only increased electrical conductivity with the produced sulfur vacancies also suppressed the increase of thermal conductivity by the lattice and/or microstructure defects (fig. 4e).

The negative values of Seebeck coefficient (α, fig. 4b) also indicate that all the samples are n-type and the major carrier is electron. The Seebeck coefficient decreases with carrier concentration (n) and carrier mobility (μ) increasing according to Mott expression:[14]

$$\alpha = \frac{\pi^2 k_B^2}{3q}T\left\{\frac{1}{n}\frac{dn(E)}{dE} + \frac{1}{\mu}\frac{d\mu(E)}{dE}\right\}_{E=E_F} \qquad (3)$$

Combined with equation (2), α values decrease with x increasing at low temperature. For semiconductor, the carrier concentration increases and carrier mobility decreases with temperature increasing, which have the opposite effects on α, and this effect depends on the temperature and x. Fig. 4b reveals that the α value decreased first and then increased with temperature after x>1.0 and the change temperature decreased with x increasing. Owing to more lattice and/or microstructure defects scattered the carriers, the carrier mobility played a more important role on the α value for the sample of x=2.0. A significantly higher power factor is obtained from the sample of x=1.0 (fig. 4c) due to the improved electrical conductivity and modest Seebeck coefficient.
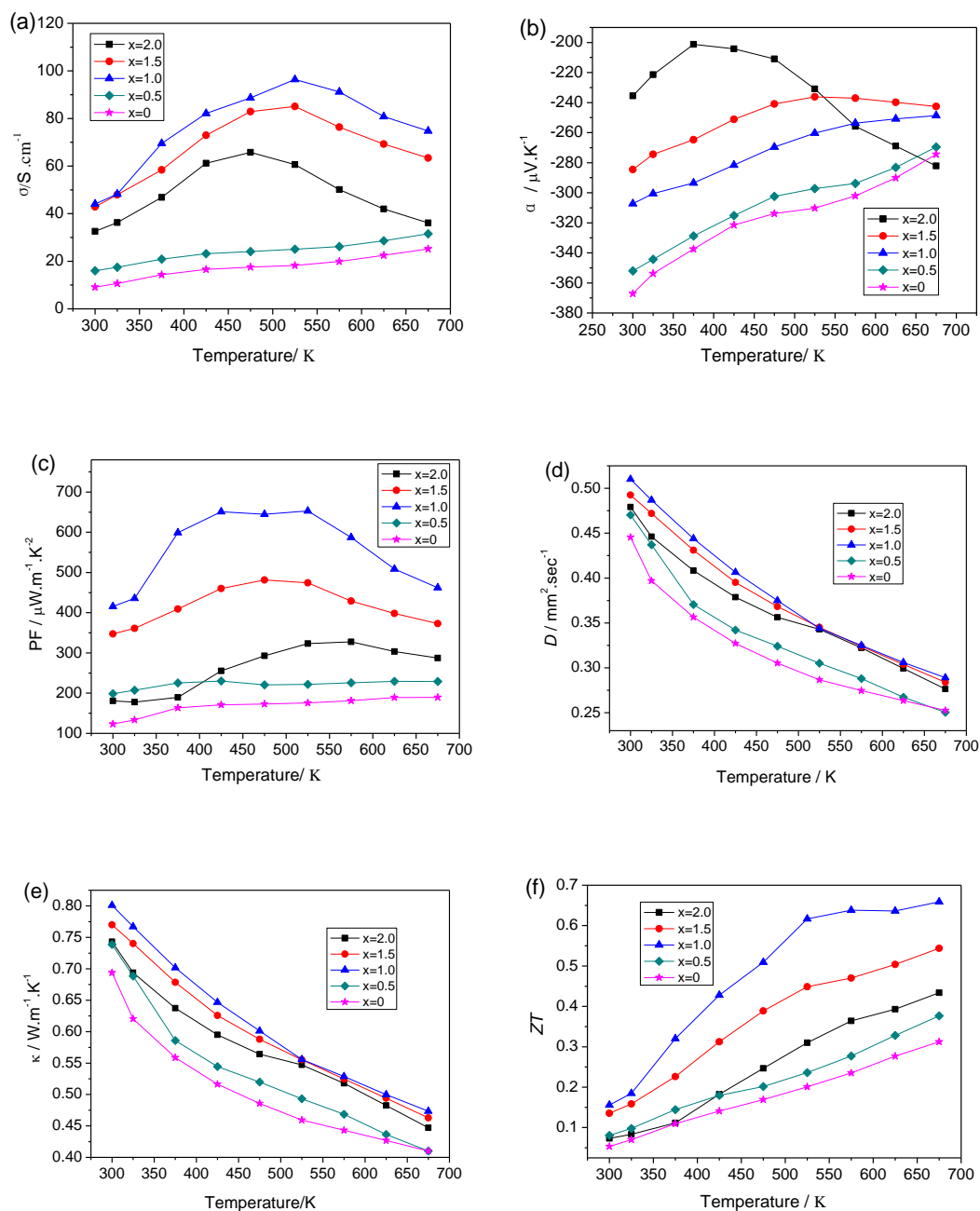
Fig. 4 Temperature dependence of electric resistivity (a), Seebeck coefficient (b), power factor (c), thermal diffusivity (d), thermal conductivity (e) and *ZT* value (f) for sintered bulk samples of Bi$_2$S$_3$ added with *x* mol% ZnO (*x*=0, 0.5, 1.0, 1.5, 2.0)

Fig. 4d, e shows the thermal diffusivity (*D*) and thermal conductivity (κ) as a function of measuring temperature for sintered samples of Bi$_2$S$_3$ added with *x* mol% ZnO (*x*=0, 0.5, 1.0, 1.5, 2.0), the κ value was calculated from the equation κ = DC_pd. The measured density values (*d*) of

Bi_2S_3 added with x mol% ZnO (x=0, 0.5, 1.0, 1.5, 2.0) are 6.469, 6.49, 6.523, 6.493 and 6.441 g.cm^{-3} respectively. The indirectly measured C_p values using standard sample (Inconel) were almost similar for all samples with and without ZnO, therefore, the C_p value of sample Bi_2S_3 (x=0) was used for all the samples in this article. The thermal conductivity for all the samples in fig. 4e decreases with increasing temperature, indicating the dominant mechanism of the phonon scattering. The low thermal conductivity of all the samples thanks to the multiple phonon scattering mechanisms by micro/nanostructures (fig. 2b-f and fig. 3) obtained from MA and SPS processes and added ZnO. From the viewpoint of percolation effect,[32] charge carriers select the low-resistivity path connected by the micrometer grains but the phonons cannot avoid the nano particles. Thus, the electrical conductivity of Bi_2S_3 added with ZnO is increased with the produced sulfur vacancies and the lattice thermal conductivity is suppressed by the lattice and/or microstructure defects. The thermal conductivity increases first and then slightly decreases with the increasing of x, which results from the inverse effect of electronic thermal conductivity and phonon scattering.

The temperature dependence of calculated ZT value is shown in fig. 4f. Combining the improved electrical conductivity, modest Seebeck coefficient and low thermal conductivity compared with the orientation ingots[9] and sub-stoichiometric Bi_2S_{3-y} bulks[5], the maximum ZT value for the sample of x=1.0 is 0.66 at 675 K. This is also an exited value for buck Bi_2S_3 system.

Conclusions

In summary, by adding ZnO to raw materials, we have developed an effective way to produce sulfur vacancy and micro/nanostructures in Bi_2S_3 during the process of MA and SPS, which efficiently enhanced the thermoelectric performance. A peak ZT value of 0.66 at 675K is reached

for Bi_2S_3 added with 1.0 % ZnO. But the exact distribution of reaction production (ZnS and SO_2) needs further investigation. If the distribution of inclusions and reaction resultants can be precisely controlled, the *ZT* value of Bi_2S_3 system should be increased to a new higher value. Furthermore, this strategy can be extended to other n-type sulfide thermoelectric materials (such as PbS) and other metal oxides usually used for desulfurization agent (such as CaO, CuO, FeO) are likely used in this method, which may be an interesting research topic in the future.

Acknowledgement

References

1. A. Cantarero, J. Martinezpastor, A. Segura and A. Chevy, *Phys Rev B*, 1987, **35**, 9586-9590.
2. B. X. Chen, C. Uher, L. Iordanidis and M. G. Kanatzidis, *Chem Mater*, 1997, **9**, 1655-1658.
3. S. C. Liufu, L. D. Chen, Q. Yao and C. F. Wang, *Applied Physics Letters*, 2007, **90**.
4. H. Mizoguchi, H. Hosono, N. Ueda and H. Kawazoe, *J Appl Phys*, 1995, **78**, 1376-1378.
5. L. D. Zhao, B. P. Zhang, W. S. Liu, H. L. Zhang and J. F. Li, *J Solid State Chem*, 2008, **181**, 3278-3282.
6. Y. Q. Yu, B. P. Zhang, Z. H. Ge, P. P. Shang and Y. X. Chen, *Mater Chem Phys*, 2011, **131**, 216-222.
7. Z. H. Ge, B. P. Zhang, Y. Liu and J. F. Li, *Phys Chem Chem Phys*, 2012, **14**, 4475-4481.
8. Z. H. Ge, B. P. Zhang, P. P. Shang and J. F. Li, *J Mater Chem*, 2011, **21**, 9194-9200.
9. K. Biswas, L. D. Zhao and M. G. Kanatzidis, *Adv Energy Mater*, 2012, **2**, 634-638.
10. L. E. Bell, *Science*, 2008, **321**, 1457-1461.
11. M. Zebarjadi, B. L. Liao, K. Esfarjani, M. Dresselhaus and G. Chen, *Adv Mater*, 2013, **25**, 1577-1582.
12. G. J. Snyder and E. S. Toberer, *Nat Mater*, 2008, **7**, 105-114.
13. V. Y. Irkhin Y. P. Irkhin, *Electronic Structure, Correlation Effects and Physical Properties of d- And f-Metals and Their Compounds*, Cambridge Int. Science Publishing, UK, 2007, pp. 57-69.
14. J. P. Heremans, V. Jovovic, E. S. Toberer, A. Saramat, K. Kurosaki, A. Charoenphakdee, S. Yamanaka and G. J. Snyder, *Science*, 2008, **321**, 554-557.
15. J. P. Heremans, B. Wiendlocha and A. M. Chamoire, *Energ Environ Sci*, 2012, **5**, 5510-5530.
16. Y. Z. Pei, H. Wang and G. J. Snyder, *Adv Mater*, 2012, **24**, 6125-6135.
17. C. M. Jaworski, V. Kulbachinskii and J. P. Heremans, *Phys Rev B*, 2009, **80**.
18. Y. Z. Pei, X. Y. Shi, A. LaLonde, H. Wang, L. D. Chen and G. J. Snyder, *Nature*, 2011, **473**, 66-69.
19. B. Poudel, Q. Hao, Y. Ma, Y. C. Lan, A. Minnich, B. Yu, X. A. Yan, D. Z. Wang, A. Muto, D. Vashaee, X. Y. Chen, J. M. Liu, M. S. Dresselhaus, G. Chen and Z. F. Ren, *Science*, 2008, **320**, 634-638.

20. K. Biswas, J. Q. He, I. D. Blum, C. I. Wu, T. P. Hogan, D. N. Seidman, V. P. Dravid and M. G. Kanatzidis, *Nature*, 2012, **489**, 414-418.

21. H. J. Wu, J. Carrete, Z. Y. Zhang, Y. Q. Qu, X. T. Shen, Z. Wang, L. D. Zhao and J. Q. He, *Npg Asia Mater*, 2014, **6**.

22. L. D. Zhao, S. H. Lo, J. Q. He, H. Li, K. Biswas, J. Androulakis, C. I. Wu, T. P. Hogan, D. Y. Chung, V. P. Dravid and M. G. Kanatzidis, *J Am Chem Soc*, 2011, **133**, 20476-20487.

23. M. Schwall and B. Balke, *Phys Chem Chem Phys*, 2013, **15**, 1868-1872.

24. H. J. Wu, L. D. Zhao, F. S. Zheng, D. Wu, Y. L. Pei, X. Tong, M. G. Kanatzidis and J. Q. He, *Nat Commun*, 2014, **5**.

25. Y. C. Zhang, T. Day, M. L. Snedaker, H. Wang, S. Kramer, C. S. Birkel, X. L. Ji, D. Y. Liu, G. J. Snyder and G. D. Stucky, *Adv Mater*, 2012, **24**, 5065-5070.

26. L. D. Zhao, V. P. Dravid and M. G. Kanatzidis, *Energ Environ Sci*, 2014, **7**, 251-268.

27. L. Dloczik, R. Engelhardt, K. Ernst, S. Fiechter, I. Sieber and R. Konenkamp, *Applied Physics Letters*, 2001, **78**, 3687-3689.

28. L. Dloczik, R. Engelhardt, K. Ernst, M. C. Lux-Steiner and R. Konenkamp, *Sensor Actuat B-Chem*, 2002, **84**, 33-36.

29. P. M. Sirimanne, K. Takahashi, N. Sonoyama and T. Sakata, *Sol Energ Mat Sol C*, 2002, **73**, 175-187.

30. T. Kosmac, D. Maurice and T. H. Courtney, *J Am Ceram Soc*, 1993, **76**, 2345-2352.

31. C. Wood, *Rep Prog Phys*, 1988, **51,** 459-539.

32. J. F. Li, W. S. Liu, L. D. Zhao and M. Zhou, *Npg Asia Mater*, 2010, **2**, 152-158.